Tunnelling effects for acoustic waves in slowly varying axisymmetric flow ducts

R.B. Nielsen[a], N. Peake[b]

[a]*Department of Mechanical and Manufacturing Engineering, Aalborg University, Fibigerstraede 16, 9220 Aalborg, Denmark*
[b]*Department of Applied Mathematics and Theoretical Physics, University of Cambridge, Wilberforce Road, CB3 0WA, United Kingdom*

Abstract

The multiple-scales Wentzel-Kramers-Brillouin (WKB) approximation is used to model the propagation of acoustic waves in an axisymmetric duct with a constriction in the presence of mean flow. An analysis of the reflection/transmission process of modes tunnelling through the constriction is conducted, and the key mathematical feature is the presence of two turning points, located at either real axial locations or in the complex plane. The resulting asymptotic solution consists of WKB solutions in regions away from the constriction and an inner solution valid in the near vicinity of the constriction. A solution which is uniformly valid throughout the duct is also derived. A range of test cases are considered, and the importance of accounting for the inner region, even in cases in which the turning points lie away from the real axis, is demonstrated.

Keywords: Non-uniform acoustic duct, tunnelling effects, turning point analysis, uniformly valid solution

1. Introduction

The interest in reducing noise emission from machinery such as aircraft engines has resulted in a considerable effort directed towards studying sound transmission through flow ducts. In many cases these ducts are axially non-uniform, but their properties vary relatively slowly with distance along the

Email address: rn@m-tech.aau.dk (R.B. Nielsen)

duct, and this allows asymptotic analysis to be used to derive simplified solutions. In this direction a key advance was made by Rienstra [1], who considered a circular lined duct with a mean flow with the duct radius varying slowly along the axis. Since then a number of extensions have been made, including to ducts of arbitrary cross section with mean flow [2], ducts with a mean swirling flow [3], curved ducts [4] and ducts carrying axially-sheared vortical mean flow [5]. In each of these papers formulae for both the local axial wave numbers and the axial variation of the modal amplitudes are derived using the Wentzel-Kramers-Brillouin (WKB) approximation.

The WKB analysis of modal propagation along a slowly-varying duct breaks down and becomes singular when the mode undergoes a transition from cut-on to cut-off, at a so-called turning point. Several of the above-mentioned references consider the case of a single turning point, and show that an incident wave is fully reflected with a phase shift $-\pi/2$, so that only an evanescent wave is transmitted beyond the turning point. In this case the solution in an inner region around the turning point is governed by Airy's equation. Multiple turning points are possible, however, and a typical scenario might involve a duct with a constriction in which, over a particular frequency range, a cut-on incident mode becomes cut-off as it approaches the constriction but then becomes cut-on again once the constriction is passed (i.e. two turning points). If these two turning points are close together then the flow in the inner region containing the turning points is governed by the parabolic cylinder equation, and the incident wave 'tunnels' through the inner region and is partially transmitted. This situation is entirely analogous to the solution of Schrödinger's equation for scattering by a parabolic potential. This latter problem was considered by Keller [6], who derived both expressions for the reflection and transmission coefficients and a uniformly-valid approximation which is valid in the vicinity of, and far away from, the turning points.

Ovenden [7] has found a uniformly-valid solution, in the style of [6], for modes undergoing a cut-on to cut-off transition at a single turning point in a slowly-varying duct with mean flow. However, the case of two nearby turning points, both in terms of determining the reflection and transmission coefficients and in terms of deriving a uniformly-valid solution, has not been completed in the acoustic-flow case, and this is therefore the focus of the current paper. As we will see, the presence of the two turning points can have a very marked effect on the acoustic propagation, even in cases when the turning points are complex and are no longer present in the flow domain.

The paper is set out as follows. In Section 2 the equations governing the flow and acoustic field are presented. The slowly varying modes, i.e. those that are either well cut-on or those far away from the transition points, are presented in Section 3. In Section 4 the wave motion through the duct constriction is studied, and reflection and transmission coefficients are determined. A uniformly-valid approximation is derived in Section 5. Specimen results are presented in Section 6.

2. Problem formulation

We adopt much of the formulation and notation used by [1, 7]. The duct has a hollow circular cross-section of axially-varying radius, and we shall focus for definiteness on the case in which the duct has a single constriction, as indicated in Figure 1. The duct walls are modelled as being perfectly rigid. There is a steady mean flow, which is purely axial and uniform in the parallel sections of the duct at infinity. The acoustic medium is assumed to be compressible, inviscid and isentropic. In what follows we non-dimensionalise distance by the duct radius far upstream, R_∞, and speed and density by the sound speed and density in the undisturbed fluid, c_∞ and ρ_∞, respectively. We introduce the axial coordinate x and polar coordinates r, θ in the cross-section of the duct. The radius of the duct is assumed to be slowly varying in the axial direction, and we introduce a slow scale, $X = \epsilon x$, where $\epsilon \ll 1$ is a measure of the axial slope of the duct walls. The local duct radius is denoted by $R = R(X)$. An acoustic wave propagates along the duct in the positive X direction, and potentially becomes cut-off as it approaches the constriction, resulting in a wave reflected back up the duct and a transmitted wave on the far side of the constriction - see Figure 1. We shall conduct the derivation with a positive going flow for convenience, but shall later alter the flow direction by a sign change.

The total flow field is decomposed into a mean flow plus a small time-harmonic perturbation [1],

$$[\tilde{\mathbf{v}}, \tilde{\rho}, \tilde{p}, \tilde{c}] = [\mathbf{V}, D, P, C] + [\nabla\phi, \rho, p, c]\, \mathrm{e}^{-\mathrm{i}\omega t} \ , \tag{1}$$

where $\tilde{\mathbf{v}}$ is the total velocity field and $\tilde{\rho}, \tilde{p}, \tilde{c}$ are the total density, pressure and sound speed. Capital letters denote mean quantities. The flow field is governed by the equations of mass and momentum conservation, together

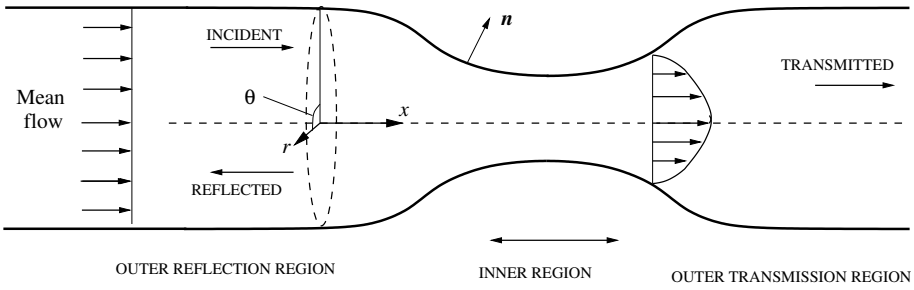

Figure 1: Illustration of the duct with a constriction. Sound is incident from the left.

with the isentropic relationships [8]

$$\tilde{c}^2 = \tilde{\rho}^{\gamma-1} \tag{2}$$

$$\gamma\tilde{p} = \tilde{\rho}^{\gamma} \ , \tag{3}$$

where γ is the ratio of specific heats. Note that in (1) the velocity perturbation is irrotational, thanks to the incident perturbation being an acoustic wave. This allows the introduction of the unsteady velocity potential, ϕ, which satisfies the convected wave equation [1]

$$\nabla \cdot (D\nabla\phi) - D\left(-\mathrm{i}\omega + \mathbf{V}\cdot\nabla\right)\left[\frac{1}{C^2}\left(-\mathrm{i}\omega + \mathbf{V}\cdot\nabla\right)\phi\right] = 0 \ . \tag{4}$$

For our hard-walled duct the steady and unsteady boundary conditions are

$$\mathbf{V}\cdot\mathbf{n} = \nabla\phi\cdot\mathbf{n} = 0 \quad \text{ on } R = R(X) \ , \tag{5}$$

where $\mathbf{n}$ is the outward-pointing wall normal vector. Following [1], the steady mean flow component can be expanded as

$$\mathbf{V}(X,r,\theta) = U_0(X)\mathbf{e}_x + \epsilon V_1(X,r)\mathbf{e}_r + O(\epsilon^2) \tag{6}$$

$$D(X,r) = D_0(X) + O(\epsilon^2) \tag{7}$$

$$C(X,r) = C_0(X) + O(\epsilon^2) \tag{8}$$

$$P(X,r) = P_0(X) + O(\epsilon^2) \ , \tag{9}$$

where V_1 is the mean velocity in the radial direction. The leading-order mean flow components can be determined from Bernoulli's equation, mass flux conservation, and the isentropic equations (2) and (3). The asymptotic solution to equation (4), and hence for the unsteady flow, will be derived in the next section.

3. The unsteady flow and slowly varying duct modes

The WKB solution for the unsteady flow has been derived in [1], and we will only present those details here which are required for our turning-point analysis. We seek an asymptotic solution of (4) of the Fourier-WKB form

$$\phi \sim \left(\Phi_0 + \epsilon\Phi_1 + O(\epsilon^2)\right) \mathrm{e}^{\frac{\mathrm{i}}{\epsilon}\int^X k(X')\mathrm{d}X' + \mathrm{i}m\theta}, \tag{10}$$

where m is the (given) integer azimuthal order and $k(X)$ is the (unknown) slowly-varying axial wave number. Inserting (10) into (4) and collecting terms of $O(1)$ yields the Bessel equation

$$\frac{\partial^2\Phi_0}{\partial r^2} + \frac{1}{r}\frac{\partial\Phi_0}{\partial r} + \left(\frac{(\omega - kU_0)^2}{C_0^2} - k^2 - \frac{m^2}{r^2}\right)\Phi_0 = 0\,, \tag{11}$$

while the $O(1)$ unsteady boundary condition becomes

$$\frac{\partial\Phi_0}{\partial r} = 0 \quad \text{on} \quad r = R(X)\,. \tag{12}$$

We write $\Phi_0 = N(X)\psi(r;X)$, where

$$\psi = J_m(\alpha r)\,, \tag{13}$$

and $\alpha = \frac{\mu_j}{R(X)}$, with μ_j being the jth root of $J'_m(\mu_j) = 0$ in order to satisfy the $O(1)$ boundary condition. The axial wave number is found to be

$$k = \frac{-\omega U_0}{C_0^2 - U_0^2} \pm \frac{\omega C_0\sigma}{C_0^2 - U_0^2}\,, \tag{14}$$

where $\pm$ denote modes propagating in the positive and negative X directions respectively, and σ is the reduced wave number

$$\sigma = \sqrt{1 - (C_0^2 - U_0^2)\,\frac{\alpha^2}{\omega^2}}\,. \tag{15}$$

The unknown amplitude $N(X)$ varies slowly in the axial direction, and is found from the solvability condition at $O(\epsilon)$. The $O(\epsilon)$ terms in (4) are

$$\begin{aligned}&\frac{\partial^2\Phi_1}{\partial r^2} + \frac{1}{r}\frac{\partial\Phi_1}{\partial r} + \left(\frac{(\omega - kU_0)^2}{C_0^2} - k^2 - \frac{m^2}{r^2}\right)\Phi_1 = \\ &-\frac{\mathrm{i}}{\Phi_0}\left\{\frac{\partial}{\partial X}\left[\left(\frac{(\omega - kU_0)U_0}{C_0^2} + k\right)D_0\Phi_0^2\right] + \frac{1}{r}\frac{\partial}{\partial r}\left[rV_1\frac{\omega - kU_0}{C_0^2}D_0\Phi_0^2\right]\right\}\,,\end{aligned} \tag{16}$$

with the $O(\epsilon)$ boundary condition

$$\frac{\partial \Phi_1}{\partial r} + \mathrm{i}kR'\Phi_0 = 0 \quad \text{on} \quad r = R(X)\,, \tag{17}$$

where $'$ denotes differentiation with respect to argument. Equations (16) and (17) can be combined to yield the transport equation

$$\frac{\mathrm{i}}{N}\frac{\mathrm{d}}{\mathrm{d}X}\left[\frac{\omega\sigma D_0 R^2}{C_0}N^2\right] = 0\,, \tag{18}$$

and providing we do not cross a point where $\sigma(X)$ is zero, we find that, apart from a multiplicative constant, $N(X)$ is given by

$$N(X) = \sqrt{\frac{C_0(X)}{\omega\sigma(X)D_0(X)R^2(X)}}\,. \tag{19}$$

The corresponding unsteady potential is given by

$$\begin{aligned}\phi =& \sqrt{\frac{C_0(X)}{\omega\sigma(X)D_0(X)R^2(X)}}J_m\left(\frac{\mu_j}{R(X)}r\right)\mathrm{e}^{\mathrm{i}m\theta}\mathrm{e}^{-\frac{\mathrm{i}}{\epsilon}\int^X \frac{\omega U_0}{C_0^2-U_0^2}\mathrm{d}X'} \\ & \left\{\beta_1\mathrm{e}^{\frac{\mathrm{i}}{\epsilon}\int^X \frac{\omega C_0\sigma}{C_0^2-U_0^2}\mathrm{d}X'} + \beta_2\mathrm{e}^{-\frac{\mathrm{i}}{\epsilon}\int^X \frac{\omega C_0\sigma}{C_0^2-U_0^2}\mathrm{d}X'}\right\}\,,\end{aligned} \tag{20}$$

where $\beta_{1,2}$ are at this stage arbitrary constants denoting amplitudes of waves propagating in the positive and negative X directions respectively.

The key point of our analysis is that the reduced wave number $\sigma(X)$ can indeed become zero, at so-called turning points, where equations (19) and (20) break down. We will be interested in the case in which there are two turning points in close proximity to each other, and from now on we will specialise our analysis to the case in which the slowly-varying duct possesses a constriction which is symmetric about $X = 0$ (so that $X = 0$ is the point of minimum radius). Equations (19) and (20) will then be valid in outer regions, while the turning points will lie in an inner region (of size to be determined) around $X = 0$ - see Figure 1. In the reflection outer region, where the field is made up of the incident and reflected waves, the constants in (19) are $\beta_2 = \mathcal{I}$ and $\beta_1 = \mathcal{R}$, while in the transmission region, where the field is made up of just the transmitted wave, $\beta_1 = \mathcal{T}$ and $\beta_2 = 0$. Here $\mathcal{T}$ and $\mathcal{R}$ are the (as yet unknown) transmission and reflection coefficients. In the next section we will analyse the inner region close to the turning points, with the aim of finding $\mathcal{T}/\mathcal{I}$ and $\mathcal{R}/\mathcal{I}$, and in the section after that we will find an expression for the unsteady field which is valid for all X.

4. Turning point analysis

The singular behaviour of the transport equation (18) at a turning point is due to us having neglected a higher-order term from (4) that becomes significant when $\sigma(X)$ approaches zero. It turns out that this term, found at $O(\epsilon^2)$, is

$$D_0 \left(1 - \frac{U_0^2}{C_0^2}\right) \frac{\partial^2 \Phi_0}{\partial X^2} \, . \tag{21}$$

We will therefore promote this term by adding (21) to (16), and then multiplying by $\Phi_0(X)$ and integrating over the duct cross section yields

$$\mathrm{i}\frac{\mathrm{d}}{\mathrm{d}X}\left[\frac{\omega\sigma D_0 R^2}{C_0} N^2(X)\right] + \epsilon R^2 D_0 \left(1 - \frac{U_0^2}{C_0^2}\right) N(X) \frac{\mathrm{d}^2 N(X)}{\mathrm{d}X^2} = 0 \, . \tag{22}$$

Note that this corrected equation is no longer singular when $\sigma = 0$, due to the introduction of the second derivative term with non-vanishing coefficient.

We shall now introduce an appropriate inner scaling that balances the terms in (22). For small X we expand the reduced wave number as

$$\sigma^2 \sim A^2(X^2 - b) \quad \text{as} \quad X \to 0 \, . \tag{23}$$

The parameter b is real, but may be positive, zero or negative, representing the cases of two real turning points placed symmetrically at $X_t = \pm\sqrt{b}$, a double turning point at $X_t = 0$, or two complex turning points at $X_t = \pm\mathrm{i}\sqrt{-b}$, respectively. We now introduce a scaled inner coordinate $\bar{X} = \epsilon^q X$ for some q, and by inspection we see that $q = -1/2$ ensures that the new term in (22) becomes of the same order as the original term. This shows that the inner region we need to consider around $X = 0$ is of size $X = O(\epsilon^{1/2})$. Furthermore, we introduce, $b = \epsilon\bar{b}$ with $\bar{b} = O(1)$, so that the turning points necessarily lie within this inner region. Making the substitution

$$N(X) = B(X)\mathrm{e}^{-\frac{\mathrm{i}}{\epsilon}\int_0^X \frac{\omega c_0 \sigma}{C_0^2 - U_0^2}\mathrm{d}X'} \, , \tag{24}$$

the rescaled transport equation in the inner region becomes

$$\frac{\mathrm{d}^2 B}{\mathrm{d}\bar{X}^2} + \left(\frac{\omega C_0}{C_0^2 - U_0^2}\right)^2 A^2 \left(\bar{X}^2 - \bar{b}\right) B = 0 \, ; \tag{25}$$

note that slowly-varying quantities such as $R(X)$ and the mean-flow properties are constant over this inner region and are therefore evaluated at $X = 0$ in (25). Further reduction of (25) to standard form is completed by introducing

$$z = \bar{X}\sqrt{2A\frac{\omega C_0}{C_0^2 - U_0^2}} \tag{26}$$

$$a = \frac{A\bar{b}}{2}\frac{\omega C_0}{C_0^2 - U_0^2}\,, \tag{27}$$

to give the *Parabolic Cylinder Equation*

$$\frac{\mathrm{d}^2 B}{\mathrm{d}z^2} + \left(\frac{z^2}{4} - a\right) B = 0\,. \tag{28}$$

This is to be compared to the case of a single isolated turning point studied in [1, 7], in which the inner solution satisfies Airy's equation. Equation (28) has the solution [9]

$$B = c_1 W(a, z) + c_2 W(a, -z)\,, \tag{29}$$

where the parabolic cylinder functions $W(a, \pm z)$ are linearly independent, and c_1 and c_2 are unknown constants to be determined.

We will now complete the matching between the inner and outer regions. First, we take the inner limit of the outer solution. For positive X, i.e. in the transmission outer region, we take the limit as X approaches the turning point at $X = \sqrt{b}$ from above, which from (20) gives

$$\phi \sim \left[\sqrt{\frac{C_0}{\omega D_0 R^2}}\right]_{X=X_t} \frac{\mathcal{T}}{A^{1/2}X^{1/2}} \mathrm{e}^{\frac{\mathrm{i}}{\epsilon}\frac{\omega C_0}{C_0^2-U_0^2}\frac{A}{2}X^2 - \mathrm{i}\frac{a}{2} - \mathrm{i}a\ln\left(\frac{2X}{\sqrt{b}}\right)} \qquad \text{as} \quad X \searrow \sqrt{b}\,. \tag{30}$$

Here we have omitted the Bessel-Fourier part of the solution as this appears similarly in both inner and outer solutions. A similar expression to (30) can be found for the inner limit of the outer solution in the reflection region, i.e. in the limit $X \nearrow -\sqrt{b}$, this time involving the reflection coefficient $\mathcal{R}$.

We now consider the outer limit of the inner expansion (28), and the appropriate expansions of $W(a, z)$ for large positive and negative arguments

are available in [9]. Taking first the limit $z \to +\infty$ we find

$$\phi \sim \left[c_1 \sqrt{\frac{\bar{k}}{2z}} - \mathrm{i} c_2 \sqrt{\frac{1}{2\bar{k}z}} \right] \mathrm{e}^{\mathrm{i}\Omega} + \left[c_1 \sqrt{\frac{\bar{k}}{2z}} + \mathrm{i} c_2 \sqrt{\frac{1}{2\bar{k}z}} \right] \mathrm{e}^{-\mathrm{i}\Omega} \,, \tag{31}$$

where

$$\Omega = \tfrac{1}{4} z^2 - a \ln(z) + \tfrac{1}{4}\pi + \tfrac{1}{2}\phi_2 \tag{32}$$

$$\phi_2 = \angle \Gamma\left(\tfrac{1}{2} + \mathrm{i}a\right) \tag{33}$$

$$\bar{k} = \sqrt{1 + \mathrm{e}^{2\pi a}} - \mathrm{e}^{\pi a} \,, \tag{34}$$

and $\angle\{\}$ denotes the phase. By now comparing (30) and (31) we see that $c_2 = \mathrm{i}\bar{k} c_1$, in order to eliminate the left-going wave in (31). A similar matching procedure between the limit of (29) as $z \to -\infty$ and the limit of (20) as $X \nearrow -\sqrt{b}$, i.e. matching between the inner region and the outer reflection region, may be established. After some algebra we find that the unknown coefficients in (29) are given by

$$\frac{c_1}{\mathcal{I}} = \left[\sqrt{\frac{C_0}{\omega D_0}} \left(\frac{\omega C_0}{C_0^2 - U_0^2} \right)^{1/4} \right]_{X = X_t} \left(\frac{8}{\epsilon A} \right)^{1/4} \frac{\bar{k}^{1/2}}{\mathrm{i}\left(1 + \bar{k}^2\right)} \mathrm{e}^{\mathrm{i}\left(-\frac{a}{2}\ln|a| + \frac{a}{2} + \frac{\pi}{4} + \frac{\phi_2}{2} \right)} \tag{35}$$

$$c_2 = \mathrm{i}\bar{k} c_1 \,, \tag{36}$$

while in the outer region the transmission and reflection coefficients turn out to be

$$\frac{\mathcal{T}}{\mathcal{I}} = \frac{\mathrm{e}^{\mathrm{i}a - \mathrm{i}a\ln|a| + \mathrm{i}\phi_2}}{\sqrt{1 + \mathrm{e}^{2a\pi}}} \tag{37}$$

$$\frac{\mathcal{R}}{\mathcal{I}} = \frac{\mathrm{e}^{\pi a} \mathrm{e}^{\mathrm{i}a - \mathrm{i}a\ln|a| + \mathrm{i}\phi_2 - \mathrm{i}\pi/2}}{\sqrt{1 + \mathrm{e}^{2a\pi}}} \,. \tag{38}$$

By taking the limit $a \to \infty$ (which is equivalent to taking $\bar{b} \to \infty$, or allowing the $O(\epsilon)$ parameter b to become $O(\epsilon)$, so that the adjacent turning points are more apart and out of the inner region) and noting that $\phi_2 \sim a \ln|a| - a$ for large $|a|$, we find from (37) and (38) that $\frac{\mathcal{T}}{\mathcal{I}} \to 0$ and $\frac{\mathcal{R}}{\mathcal{I}} \to \exp(-\mathrm{i}\pi/2)$. As expected, the usual isolated turning point result is therefore regained in the limit of very large tunnelling distance (note that other authors, e.g. [1, 7]

quote that the reflection coefficient at an isolated turning point is $\exp(\mathrm{i}\pi/2)$, but this difference results only from our alternative choice of sign convention $\exp(-\mathrm{i}\omega t)$). In contrast, in the limit $a \to -\infty$ (i.e. b becomes $O(1)$ and negative), so that the turning points are imaginary and located far from the real axis, we find $\frac{\mathcal{T}}{\mathcal{I}} \to 1$ and $\frac{\mathcal{R}}{\mathcal{I}} \to 0$. This corresponds to the wave propagating essentially straight through the constriction, with only exponentially small reflection. In the special case $a = 0$, which is when the two turning points merge, $\left|\frac{\mathcal{T}}{\mathcal{I}}\right| = \left|\frac{\mathcal{R}}{\mathcal{I}}\right| = \frac{1}{\sqrt{2}}$, so that we have equipartition of incident energy between the transmitted and reflected waves. Specimen results for $\mathcal{R}/\mathcal{I}$ and $\mathcal{T}/\mathcal{I}$ are given in Figure 2 in the case of nonzero flow described in more detail in section 6, and the features mentioned earlier in this paragraph are clearly visible.

We have now found the solution for the unsteady flow field in the inner and outer regions separately. This solution is not entirely satisfactory, however, because if we wish to compute the solution anywhere in the flow then we are faced with the issue that the outer solution (20) is singular in the neighbourhood of the turning points. In the next section we will therefore follow [7] for the single turning point problem and derive a uniformly-valid solution for the unsteady flow, which can be used to evaluate the unsteady flow anywhere in the duct.

5. Uniformly-valid solution

We will now derive an asymptotic solution for the unsteady flow which is uniformly valid all along the duct. This was done by Ovenden in [7] for a flow duct with a single turning point, using the replacement variable method of Ludwig and Kravtsov [10, 11]. The solution we present here parallels the work of Keller [6], who derived a uniformly-valid approximation for the closely-related problem of scattering by a potential barrier for the Schrödinger equation.

We start with just the terms which are formally $O(1)$ in (4) for slowly-varying mean flow, i.e.

$$\left(1 - \frac{U_0^2}{C_0^2}\right)\frac{\partial^2\phi}{\partial x^2} + \frac{2\mathrm{i}\omega U_0}{C_0^2}\frac{\partial\phi}{\partial x} + \left(\frac{\omega^2}{C_0^2} - \alpha^2\right)\phi = 0 \,, \tag{39}$$

which is reduced to the standard form

$$\frac{\partial^2\tilde{\phi}}{\partial x^2} + k_2^2\tilde{\phi} = 0 \tag{40}$$

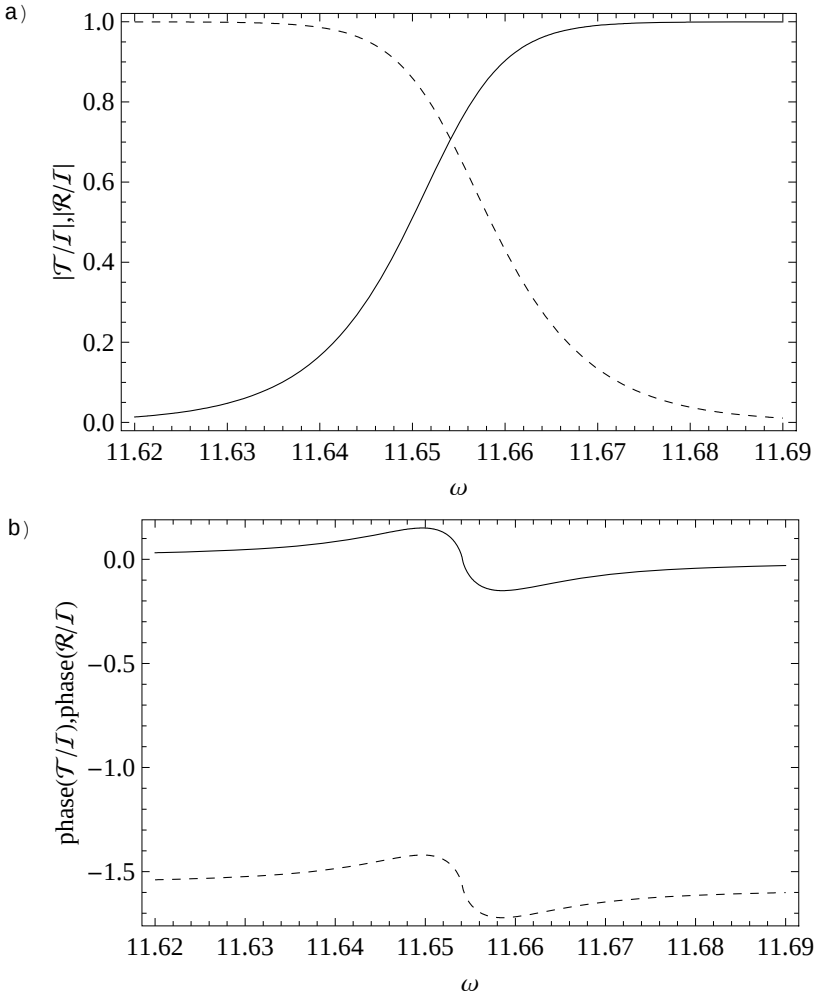

Figure 2: Variation of *a)* the amplitude and *b)* the phase of the reflection (dashed line) and transmission (solid line) coefficients $\mathcal{R}/\mathcal{I}$ and $\mathcal{T}/\mathcal{I}$ with frequency. Conditions are for the flow case described in section 6.

with $k_2 = \frac{\omega C_0 \sigma}{C_0^2 - U_0^2}$ by the substitution

$$\phi = \tilde{\phi} \mathrm{e}^{-\mathrm{i} \int \frac{U_0 \omega}{C_0^2 - U_0^2} \mathrm{d}x} \ . \tag{41}$$

Note that $O(\epsilon)$ terms arising from derivatives of slowly varying quantities which arise in deriving (39) from the wave equation (4). Following [6] we seek a solution to (40) of the form

$$\tilde{\phi} = \Phi(X, r, \theta) \frac{G(\zeta)}{(\zeta_x)^{1/2}} \ , \tag{42}$$

where $\zeta(x)$ is a function to be determined but which we assume to be such that its derivative ζ_x is a function of only the slow coordinate X. With this substitution (40) becomes, to leading order,

$$\left(G'' + \frac{k_2^2}{\zeta_x^2} G \right) = 0 \ . \tag{43}$$

We now choose ζ so that (43) is the parabolic cylinder equation (28). This requires

$$\zeta_x^2 \left(\frac{\zeta^2}{4} - \eta \right) = k_2^2 \ , \tag{44}$$

and then

$$G(\zeta) = h_1 W(\eta, \zeta) + h_2 W(\eta, -\zeta) \tag{45}$$

with η as the (as yet unknown) parameter corresponding to a in equation (28). Note that the turning points occur when $k_2 = 0$, and from (44) this is equivalent to $\zeta^2 = 4\eta$.

The next step is to determine the relationship between ζ and x by integrating (44), and the result will depend on whether the two turning points either lie on the real axis or form a complex conjugate pair. First, for two real turning points, say $x = \pm\sqrt{b}/\epsilon$, we have $\zeta(\pm\sqrt{b}/\epsilon) = \pm 2\sqrt{\eta}$ with $\eta > 0$. Integrating equation (44) separately in the three portions of the x axis delineated by the turning points then yields: for $x > \sqrt{b}/\epsilon$

$$\frac{\zeta}{4} \sqrt{\zeta^2 - 4\eta} - \eta \ln \left[\frac{\zeta + \sqrt{\zeta^2 - 4\eta}}{2\eta} \right] = \int_{\sqrt{b}/\epsilon}^{x} k_2 \mathrm{d}x \ ; \tag{46}$$

for $-\sqrt{b}/\epsilon < x < \sqrt{b}/\epsilon$

$$\frac{\zeta}{4}\sqrt{4\eta-\zeta^2}+\eta\sin^{-1}\left(\frac{\zeta}{2\sqrt{\eta}}\right)+\frac{\pi\eta}{4}=\int_{-\sqrt{b}/\epsilon}^{x}|k_2|\mathrm{d}x\ ; \tag{47}$$

and for $x < -\sqrt{b}/\epsilon$

$$\frac{\zeta}{4}\sqrt{\zeta^2-4\eta}+\eta\ln\left[\frac{-\zeta+\sqrt{\zeta^2-4\eta}}{2\eta}\right]=\int_{-\sqrt{b}/\epsilon}^{x}k_2 dx\ . \tag{48}$$

At this stage we still do not know the value of the parameter η, but by setting $\zeta(\sqrt{b}/\epsilon)=2\sqrt{\eta}$ in (47) we find

$$\pi\eta=\int_{-\sqrt{b}/\epsilon}^{\sqrt{b}/\epsilon}|k_2|\mathrm{d}x\ , \tag{49}$$

which fixes η.

Second, if the turning points are complex, at say $x=\pm\mathrm{i}\sqrt{-b}/\epsilon$, then we have $\zeta(\pm\mathrm{i}\sqrt{-b}/\epsilon)=\pm 2\sqrt{-\eta}$ with $\eta<0$ then by integrating (44) and setting $\phi=0$ at $x=0$ (recall that the duct is symmetric about $x=0$), we find

$$\frac{\zeta}{4}\sqrt{\zeta^2+4|\eta|}+|\eta|\ln\left(\frac{\zeta+\sqrt{\zeta^2+4|\eta|}}{2|\eta|^{1/2}}\right)=\int_0^x k\mathrm{d}x\ , \tag{50}$$

which is valid for any x. In order to determine η we simply set $x=\pm\mathrm{i}\sqrt{-b}/\epsilon$ successively in (50) to find

$$\pi|\eta|=\int_{-\sqrt{-b}/\epsilon}^{\sqrt{-b}/\epsilon}k(\mathrm{i}s)\mathrm{d}s\ . \tag{51}$$

In summary, we have now set out a procedure for determining $\zeta(x)$: The parameter η in the parabolic cylinder equation is determined from either equation (49) or (51), depending on whether the turning points are real or complex respectively, and then ζ is obtained as a function of x from equations (46), (47) and (48) for $\eta>0$ and from equation (50) for $\eta<0$. This naturally entails numerical integration of k and then solving for ζ numerically, but this is straightforward in all cases. Note finally that ζ_x is best determined from equation (44).

In order to complete the determination of the uniformly-valid solution we require values for the constants $h_{1,2}$ in (45) and an expression for the function $\Phi(X, r, \theta)$ in (42). We insist on no left-going wave in the transmission region, and in the same way as was done in section 4 we find $h_2 = \mathrm{i}\bar{k}h_1$. Without loss of generality we can set $h_1 = 1$, and then in order to match with the incident wave in the reflection region we set

$$\Phi(X, r, \theta) = \frac{2\sqrt{\bar{k}}\mathcal{I}}{\bar{k}^2 + 1}\sqrt{\frac{C_0^2}{D_0(C_0^2 - U_0^2)R^2}}\mathrm{e}^{\mathrm{i}m\theta}J_m(\alpha r)\mathrm{e}^{-\frac{\mathrm{i}\eta}{2}\ln(\eta)+\frac{\mathrm{i}\eta}{2}-\frac{\mathrm{i}\pi}{4}+\frac{\mathrm{i}\phi_2}{2}} \ , \quad (52)$$

having expanded the parabolic cylinder functions in equation (45) for large negative argument. The derivation of the uniform solution is therefore complete, and in the next section we will present some results.

6. Results

In what follows we will consider the duct with radius defined by

$$R(X) = 1 - 0.3\,\mathrm{sech}(X) \ . \quad (53)$$

We select $\epsilon = 0.1$, the ratio of specific heats is $\gamma = 1.4202$, and without loss of generality we set the incident amplitude $\mathcal{I} = 1$. For convenience we will consider the quantity

$$\Psi = \frac{\phi}{\mathrm{J}_m(\alpha r)\exp(\mathrm{i}m\theta - \mathrm{i}\omega t)} \ , \quad (54)$$

as well as the full unsteady potential ϕ. Results with and without mean flow will be reported.

We first consider a test case with zero mean flow. The circumferential wave number is $m = 21$ and we study the fourth radial mode (as in the zero mean flow test case of [7]). The axial variation of Ψ for three different frequencies is shown in Figure 3. In each case the mode is cut on in the parallel portions of the duct, while the locations of the two turning points are given in the figure caption. As the frequency increases the turning points are at first real (Figure 3a) but move closer together and coalesce (at $\omega \approx 52.93$, in Figure 3b), before moving off (but remaining close to) the real axis (Figure 3c). The singularities in the outer solution at the real turning points are clearly visible in Figures 3a and 3b , but note that even when the

turning points are imaginary their close proximity to the real axis in Figure 3c still leads to a (in this case small) discrepancy with the inner solution. The tunnelling effect can be clearly observed in Figure 3a as a relatively rapid decay with increasing X through the inner region, while in Figure 3c tunnelling is absent and the field is approximately symmetric in X across the inner region. In each case the maximum value of Ψ is located close to $X = 0$, but this local peak value decreases as frequency increases. At the same time, the location of the peak also drifts from just ahead of the left-most turning point towards the centre of the constriction.

In Figures 4 we compare our uniformly-valid solution with the inner and outer solutions, and note how the uniformly-valid solution is visually indistinguishable from the outer and inner solutions over the appropriate X ranges. In Figure 5 we use the uniformly-valid solution to plot a contour map of the unsteady potential throughout the duct. The localisation of the mode towards the outer duct wall is typical of the higher radial order modes with large azimuthal order. As expected, the maximum amplitude of the field in the duct is observed in the neighbourhood of the turning points.

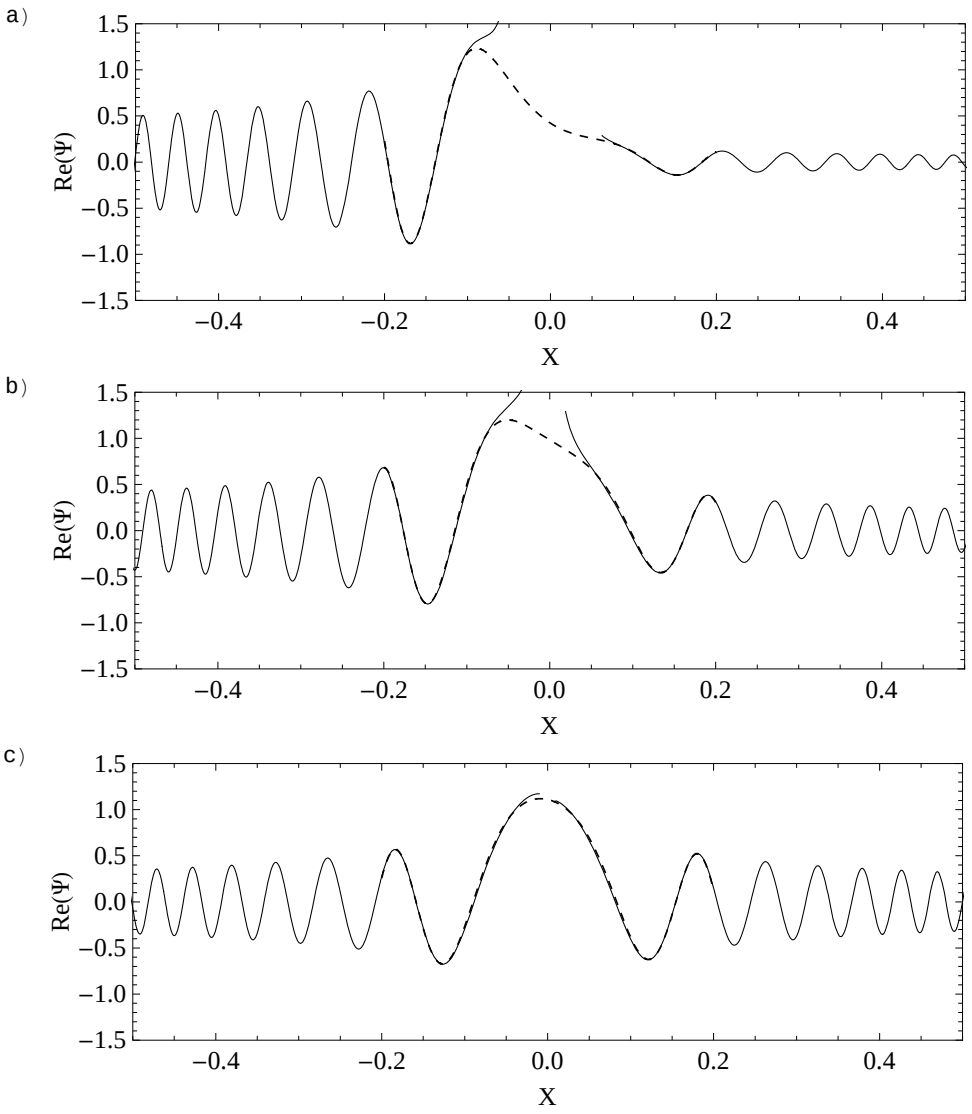

Figure 3: Axial variation of $\mathrm{Re}(\Psi)$ as a function of X, with zero mean flow. The incident mode has $m = 21$ and is the fourth radial mode. The solid lines are the outer solution and the dashed line are the inner solution. *a)* at $\omega = 52.9$ (turning points $X_t = \pm 0.052$), *b)* at $\omega = 52.93$ ($X_t = \pm 0.009$), *c)* at $\omega = 52.95$ ($X_t = \pm \mathrm{i}0.041$).

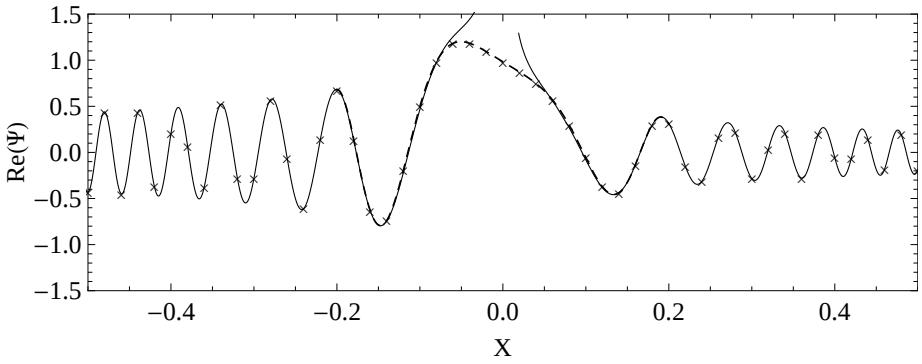

Figure 4: Comparison of uniform solution with outer and inner expansions, $\omega = 52.93$, other conditions as in Figure 3. Solid-Dashed curve: composite solution, crosses: Uniformly valid solution.

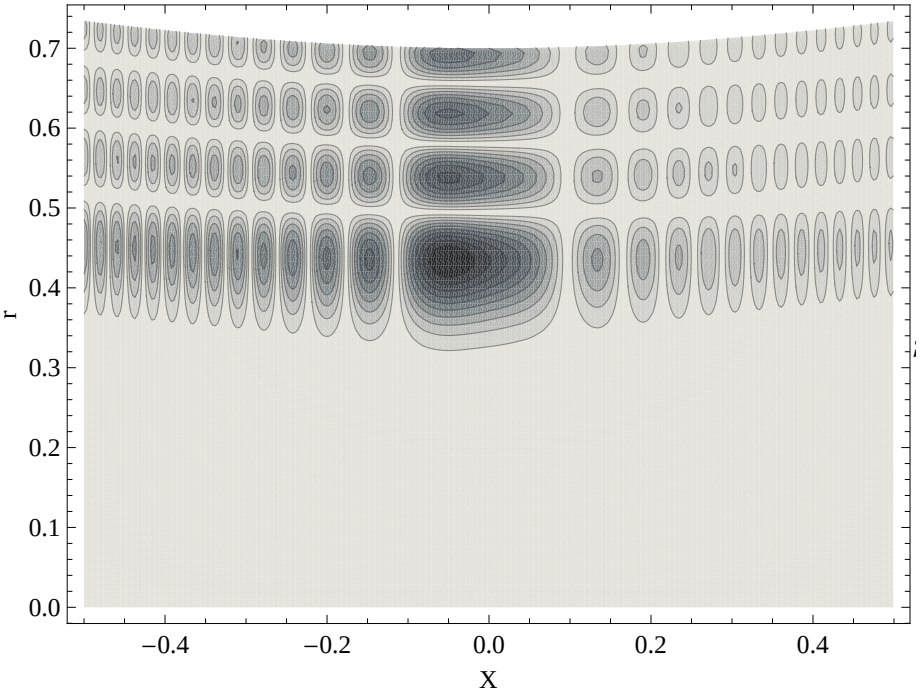

Figure 5: Contour map of $|\phi/\max(\phi)|$, conditions as in Figure 4.

We now consider a test case with mean flow by setting $U_0(\infty) = -0.2$ (the choice of a negative value means that the incident wave propagates in the upstream direction, and corresponds to the practically relevant case of noise generated by the fan travelling towards the inlet in an aeroengine). Here the circumferential wave number is $m = 4$ and we consider the second radial mode. The axial variation of Ψ is shown in Figure 6 for increasing frequency. In each case the distorted waveform in $X < 0$ arises from the interference between the reflected wave of longer wavelength and the incident wave of shorter wave length; for negative U_0 the axial wave number k is larger for propagation in the positive X direction (the + sign in equation (14)) than for propagation in the negative X direction (the − sign in equation (14)).

The uniformly-valid solution has been used to plot contour maps showing the spatial variation of $|\phi|$ in Figures 7 and 8 for $\omega = 11.635$ (two real turning points) and $\omega = 11.66$ (two imaginary turning points) respectively. The almost total reflection of the incident wave for $\omega = 11.635$ is apparent in Figure 7, while in Figure 8a we can observe a region of relatively large spatial extent over which the amplitude is significantly increased compared to the incident wave. In Figure 8b we plot the incident wave only as it propagates along the duct (with its amplitude varying due to the change in duct area and mean flow). Comparison of Figures 8a and 8b shows that there is a significant reflected wave in $X < 0$, despite the fact that the incident mode remains cut-on throughout the duct (specifically $|\mathcal{R}/\mathcal{I}| \approx 0.43$). This emphasises the importance of accounting for the presence of the turning points, even when they are not on the real X axis.

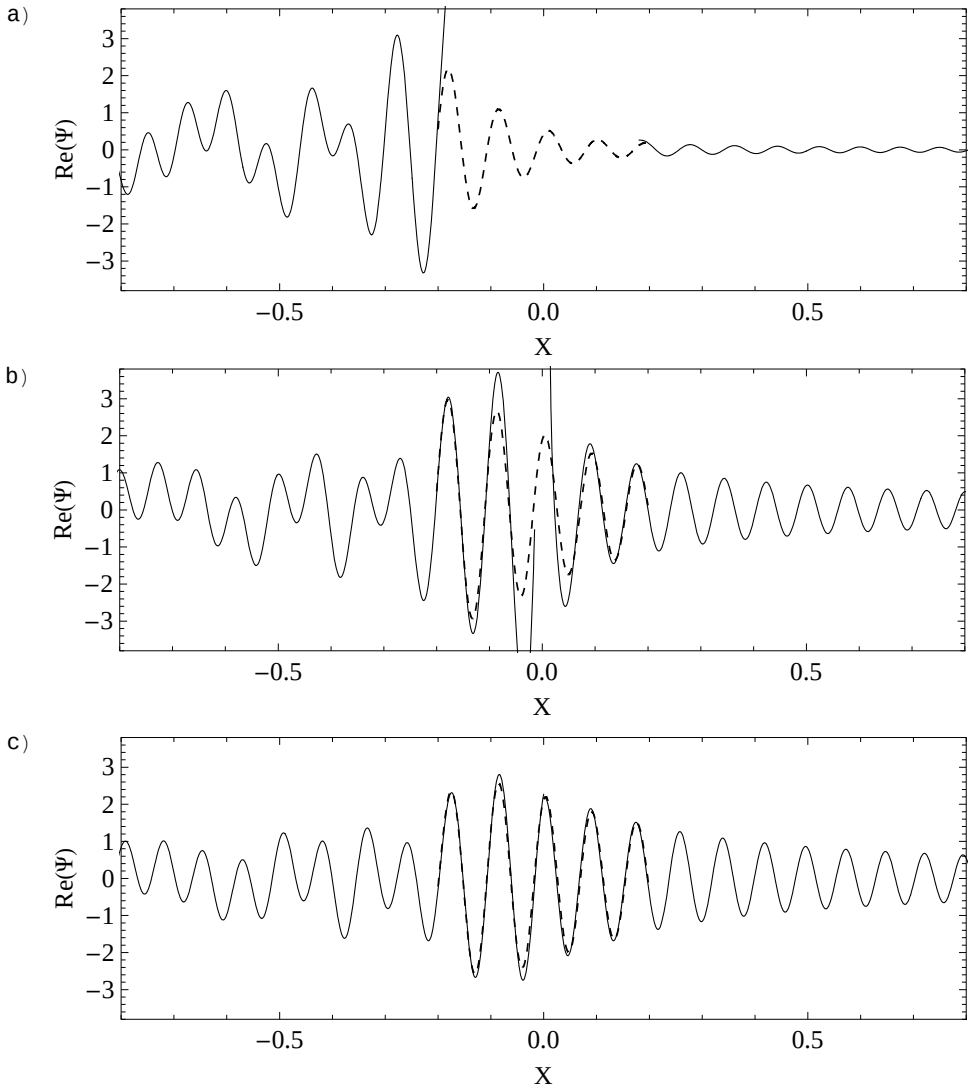

Figure 6: Axial variation of $\mathrm{Re}(\Psi)$ as a function of X, with mean flow $U_0(\infty) = -0.2$. The incident mode has $m = 4$ and is the second radial mode. The solid lines are the outer solution and the dashed line are the inner solution. *a)* at $\omega = 11.635$ ($X_t = \pm 0.18$), *b)* at $\omega = 11.654$ ($X_t = \pm 0.015$), *c)* at $\omega = 11.66$. ($X_t = \pm \mathrm{i}0.10$)

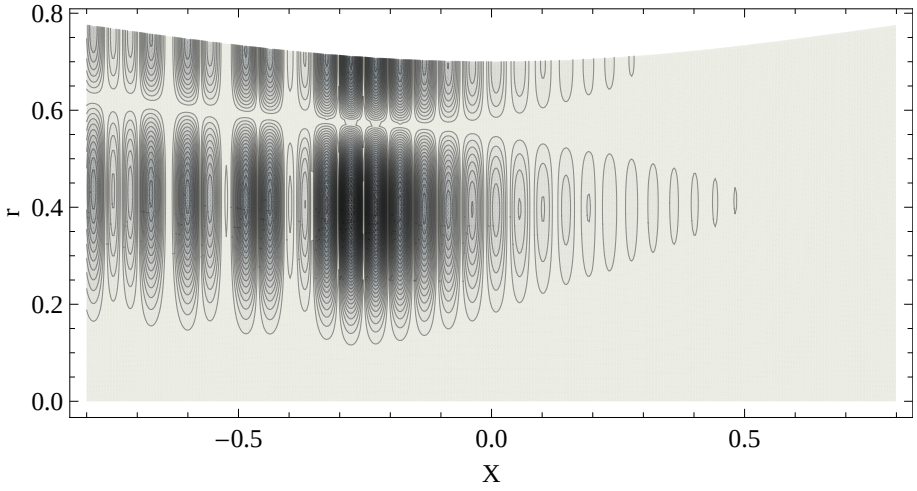

Figure 7: Contour map of $|\phi/\max(\phi)|$, with $\omega = 11.635$ and other conditions as in Figure 6. Contour levels at intervals of 1/30.

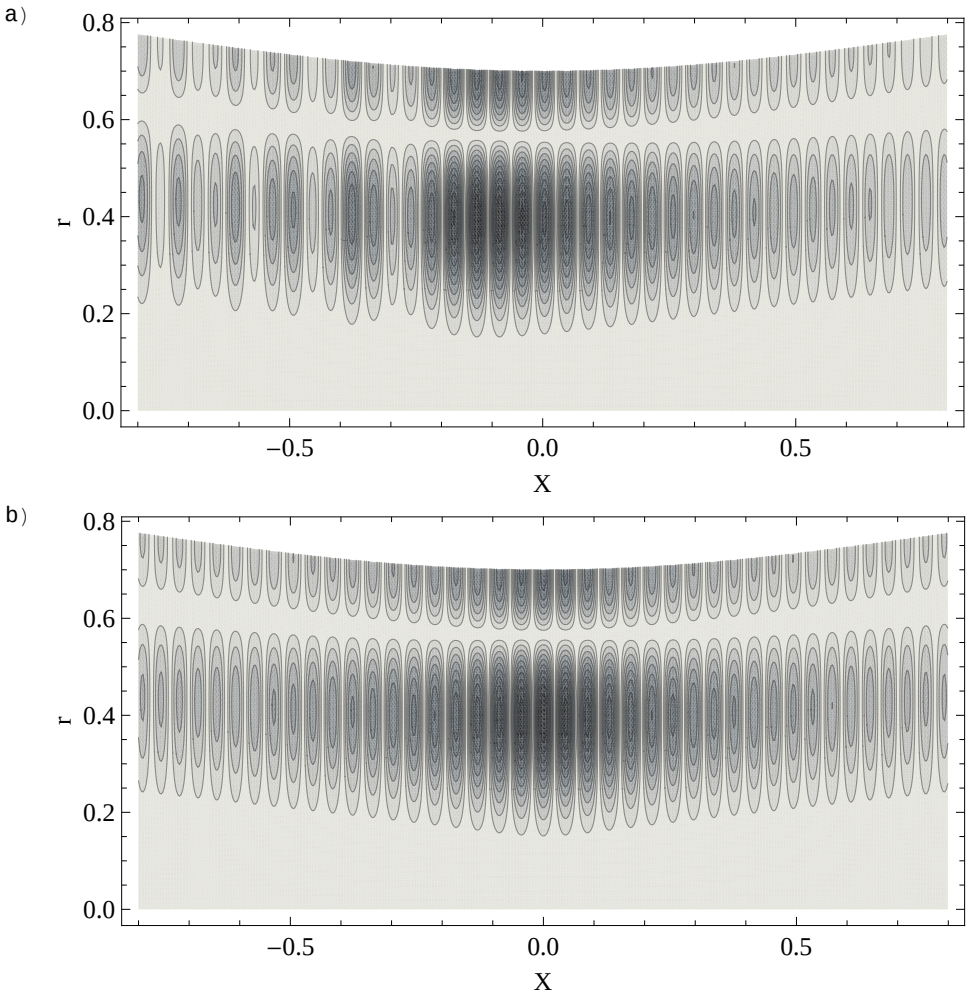

Figure 8: Contour map of $|\phi/\max(\phi)|$, with $\omega = 11.66$ and other conditions as in Figure 6. Contour levels at intervals of 0.1. In a) we show the full uniformly-valid result, while in b) we have the incident wave only.

7. Conclusions

In this paper the propagation of sound along a cylindrical flow duct with a single constriction has been studied using the WKB method, on the assumption that the duct radius varies slowly along the axis. In this case the WKB solution possesses two (potentially real) turning points, and our analysis thereby extends previous work on the isolated turning point problem for flow ducts, e.g. [1, 7]. The reflection and transmission coefficients are obtained, and we find expressions for both the WKB outer solution (which is singular at real turning points) and an inner solution valid close to the turning points. A solution which is uniformly-valid at any location in the duct is also derived, using parabolic cylinder functions in conjunction with coordinate stretching.

The effect of tunnelling is demonstrated at various frequencies with and without mean flow. In the presence of two real turning points the level of reflection from the constriction increases as the separation between the turning points increases, with the isolated turning point results recovered in the limit of large separation between the turning points. When the turning points are imaginary and lie reasonably far apart then the incident wave undergoes only very small reflection at the constriction, and the WKB solution for the incident wave only remains accurate all along the duct. However, in cases when the turning points are imaginary but lie close to the real axis we have seen that significant wave reflection is possible.

It is possible to extend our results to include a number of features such as annular ducts, more complicated mean flow (e.g. radially sheared potential flow, as in [5]) and acoustic lining (note that the inclusion of the latter necessarily has the effect of moving turning points away from the real axis, but as already noted complex turning points can still have a significant effect). It furthermore seems natural to compare such extended analysis as well as the results in this paper to numerical solutions, e.g. the finite element method, in the style of [12]. Numerical challenges seems inevitable due to the need to capture cut-off cut-on transitions, which is also identified and resolved in [12]. The existence of trapped or near-trapped modes, with consequent build-up of the local unsteady pressure amplitude, is potentially important for the structural integrity of a ducted system. For instance, [13, 14] demonstrate the possible occurrence of acoustic resonance in aeroengine intakes due to mode trapping between a turning point in the intake upstream of the fan and the swirling flow downstream of the fan. In [13, 14] only an isolated

turning point was considered, but an interesting next step would be to repeat those trapped-mode calculations using our new double turning point results. Another possible extension is concerned with the work of Smith et al [15], who showed that at high Helmholtz number a mode which goes through an isolated turning point can be scattered into other nearby cut-on modes, due to the increased modal density at high frequency. Presumably the same effect can occur in the double turning point problem as well, but detailed calculation is required to quantify this and will not be attempted here.

Acknowledgement

The research is funded by *The Danish Council for Independent Research, Technology and Production Sciences* Grant number: UK 95 OS63822 PO83004.

References

[1] S. W. Rienstra, Sound transmission in slowly varying circular and annular lined ducts with flow, Journal of Fluid Mechanics 380 (1999) 279–296, doi: 10.1017/S0022112098003607.

[2] S. W. Rienstra, Sound propagation in slowly varying lined flow ducts of arbitrary cross-section, Journal of Fluid Mechanics 495 (2003) 157–173, doi: 10.1017/S0022112003006050.

[3] A. J. Cooper, N. Peake, Propagation of unsteady distubances in slowly varying duct with mean swirling flow, Journal of Fluid Mechanics 445 (2001) 207–234, doi: 10.1017/S0022112001005559.

[4] E. Brambley, N. Peake, Sound transmission in strongly curved slowly varying cylindrical ducts with flow, Journal of Fluid Mechanics 596 (2008) 387–412, doi: 10.1017/S0022112007009603.

[5] A. Lloyd, N. Peake, The propagation of acoustic waves in a slowly varying duct with radially sheared axial mean flow, Journal of Sound and Vibration 332 (2013) 3937–3946.

[6] J. B. Keller, Uniform solutions for scattering by a potential barrier and bound states of a potential well, Am. J. Phys. 54 (6) (1986) 546–550, doi: 10.1119/1.14560.

[7] N. C. Ovenden, A uniformly valid multiple scales solution for cut-on cut-off transition of sound in flow ducts, Journal of Sound and Vibration 286 (2005) 403–416, doi: 10.1016/j.jsv.2004.12.009.

[8] A. D. Pierce, Acoustics, an Introduction to its Physical Principles and Applications, McGraw-Hill, 1981.

[9] F. W. J. Olver, D. W. Lozier, R. F. Boisvert, C. W. Clark, NIST Handbook of Mathematical Functions, Cambridge University Press, 2010.

[10] D. Ludwig, Uniform asymptotic expnasions at a caustic, Communications in Pure and Applied Mathematics 19 (1966) 215–250.

[11] Y. Kravtsov, Two new asymptotic methods in the theory of wave propagation in inhomogeneous media, Soviet Physics - Acoustics 14 (1968) 1–17.

[12] N. Ovenden, W. Eversman, S. Rienstra, Cut-on cut-off transition in flow ducts: comparing multiple-scales and finite-element solutions, AIAA Paper 2004-2945AIAA/CEAS Aeroacoustics Conference.

[13] A. J. Cooper, N. Peake, Trapped acoustic modes in aeroengine intakes with swirling flow, Journal of Fluid Mechanics 419 (2000) 151–175.

[14] A. J. Cooper, A. Parry, N. Peake, Acoustic resonance in aeroengine intake ducts, ASME Journal of Turbomachinery 126 (2004) 432–441.

[15] A. Smith, N. Ovenden, R. Bowles, Flow and geometry induced scattering of high frequency acoustic duct modes, Wave Motion 49 (2012) 109–124.